

Quantitative microarray spot profile optimization: A systematic evaluation of buffer/slide combinations

David P. Kreil*[†] Richard P. Auburn* Lisa A. Meadows* Steven Russell*
Gos Micklem*

*Department of Genetics, University of Cambridge, Downing Street,
Cambridge, CB2 3EH, U.K.

[†]Inference Group, Cavendish Laboratory, Madingley Road,
Cambridge, CB3 0HE, U.K.

Abstract

The non-trivial choice of a good combination of microarray spotting buffer and slide chemistry is critical for the reliability of microarray hybridization experiments. This choice determines the morphology of spots and, moreover, the variance of that morphology. Both strongly affect how well the extracted intensity signals correspond to sample RNA abundances. Comparisons of different buffer/slide combinations, however, have tended to be subjective, and are not suitable for a systematic approach.

Spot morphology and its variance were assessed objectively by measuring the average and variance of radial spot pixel intensity profiles. The variances assessed comprised deviations from radial symmetry and spot-to-spot reproducibility, as well as general pin-to-pin differences and slide effects. A quantitative and systematic evaluation of over 24×6 buffer / slide combinations yielded a new protocol giving superior spot profiles with minimal variance whilst also scoring excellently on other technical requirements. The process introduced here can generally be applied to evaluate new materials and technologies as they emerge.

Software is available on request from the authors. For an online supplement, please see

<http://www.inference.phy.cam.ac.uk/dpk20/spotprofiles/>.

Correspondence: D.Kreil@gen.cam.ac.uk

Introduction

Although mechanically spotted DNA microarrays have become widely used for gene expression analysis, there have been relatively few studies aimed at optimizing the various steps in a microarray experiment, even though it is known that the overall process suffers from high variability. Observed problems with reliability and reproducibility can be overcome by a combination of sophisticated data analysis and advances in experimental methods. While the exploitation of multiple measurements plays a pivotal role in many state-of-the-art approaches to analysis (Baldi and Long, 2001; Long *et al.*, 2001; Tusher *et al.*, 2001; Efron and Tibshirani, 2002; Lönnstedt and Speed, 2002; Kreil and MacKay, 2003), an efficient solution will benefit from an improved reliability of the individual measurements.

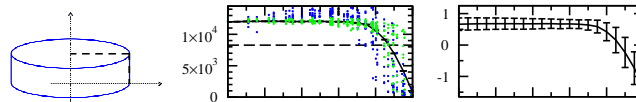


Figure 1: Radial Spot Pixel Intensity Profiles. From left to right: [1] A schematic representation of the traditional ideal spot shape. The horizontal axis shows distance from the spot centre, the vertical axis plots intensity. The radial spot profile is straight and shown by the dashed line. The mean pixel intensity used as the signal value is seen in the height of the dashed line. [2] Construction of the average and variance of a radial spot profile from a subgrid of spots. The vertical scale measures intensities of individual spot pixels vs their radial distances on the horizontal axis. The dashed line is the average signal value of all spots in the subgrid. The mean spot pixel intensity has been used as the signal value for each individual spot (see [1]). The solid line traces the subgrid Loess average. For demonstration purposes, the pixels of only two randomly chosen spots are shown. For comparison purposes, the scales give values normalized per subgrid. [3] Average and variance of a radial spot profile from a subgrid of spots. The results for the entire subgrid are shown, both the average profile shape and the Loess smoothed local variance. Note the higher variance at the spot edge, which can already be seen in the bigger spread of the raw pixel data in [2].

The quantification of a particular spot image always makes approximating assumptions about the spot morphology, i.e., the spot shape and internal structure. Typically, the intensities of all the pixels constituting a given spot are averaged to give a *signal* value assigned to the spot. Some modern spot finding tools (e.g., Yang *et al.*, 2001), select individual pixels from a spot, and then average over only those pixels. Further data processing then aims to correct for factors specific to individual slides or slide areas, like labelling and hybridization efficiencies or non-specific hybridization, ideally making the signal a good measure of the sample RNA content matching the particular probe. In all cases, some kind of a spot model is assumed, although not necessarily stated, and the pixel intensities are noisy measurements used to infer the *signal* intensity of a given spot (Brown *et al.*, 2001).

In general, an ideal spot is modelled as a flat disc (cf. Fig. 1), and the height of the disc is taken to represent the strength of the signal. Statistical models of experimentally observed spot images can be built (Balagurunathan *et al.*, 2002), which show both the systematic and the random deviations of the true spot shape from that of a flat disc. Experimentally observed spots do not, unfortunately, resemble flat discs, and their morphology is determined by a multitude of interacting parameters (materials, printing and hybridization conditions employed, ...). In the past, an exploration of these parameters has been difficult, relying largely on subjective comparisons by eye.

Here, a quantitative method to assess spot morphology and its fluctuations by radial spot pixel intensity profiles is introduced and validated in the evaluation of over 24×6 spotting buffer / slide chemistry combinations. With

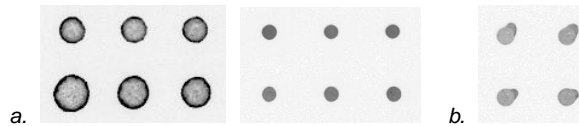


Figure 2: *a.* Rush. Heavy, 50% rush, i.e., the first printed spots are up to 50% larger than subsequent ones – 50% DMSO with 0.01% sarkosyl on PLL (left). No detectable rush – 50% DMSO with 0.1% PEG on FMB cDNA (right). *b.* Deviations from radial symmetry. Spot shape, ‘weeping spots’ – 1.5 M betaine with 10% DMSO on PLL. Spot structure – see Fig. 4.

current spot quantification methods in mind, a spot shape resembling the idealized flat disc is considered advantageous. More importantly, minimal fluctuations in spot shape make single spot measurements more robust, a benefit that will apply equally well for more elaborate spot models of the future. We present buffer / slide combinations that satisfy these criteria and also score well regarding other experimental requirements.

Systems and Methods

Full protocols are available in the Supplement.

Spotted probes – Sonicated salmon sperm DNA (Amersham, typical fragment length 1kb) was diluted to $250 \text{ ng}/\mu\text{l}$ in each spotting buffer. It should be noted that results for significantly different probe concentrations or lengths will be different, but the same methods apply. Buffers contained salt (SSC or NaPO_4) and/or DMSO, and optionally one or several additives: detergents (SDS or sarkosyl), poly-alcohols (glycerol, PEG, or PPG), and betaine. The Supplement lists all 34 spotting buffers examined (ten of which were excluded in a pilot study).

Slides tested included EZ-Aminosilane (Apogent Discoveries), CMT GAPS II and Ultra GAPS (Corning), FMB cDNA (Genetic Research Instrumentation), ArrayIt SuperAmine (TeleChem), and poly-L-lysine (PLL) slides coated in-house. For each slide type, two microarray slides were independently printed using 48 MicroSpot 2500 quill pins in a BioRobotics Micro-Grid II 600 TAS operated at $(20 \pm 2)^\circ\text{C}$ and $(60 \pm 2)\%$ relative humidity. The slide order was randomized. Each spotting buffer was printed by at least 3 randomly chosen pins. Each pin created 8×8 spots – from a single loading of buffer, to also visualize rush effects (see Fig. 2a). The inter-spot distance of $500 \mu\text{m}$ reduced the risk of merged spots.

Hybridization samples – sonicated salmon sperm DNA samples were directly labelled with Cy3-dCTP or Cy5-dCTP (Amersham, GibcoBRL).

After slide pre-processing and hybridization, all slides were scanned at 595 nm and 685 nm with an arrayWoRx Auto Biochip Reader (Applied Precision) at a resolution of $6.5040 \mu\text{m}/\text{pixel}$, ‘High SNR’ sensitivity, and 0.2 s exposure per channel, with no pixels saturating. Dapple (Buhler *et al.*, 2000) was used for image analysis.

```

QString ofn;
// cannot obtain filename from GUI here, use hard-coded path
ofn.sprintf("tmp/gx%d_gy%d_vx%d_vy%d_ch%d",
           v.gx,v.gy,v.vx,v.vy,c);
ofstream of(ofn);
// extract the foreground and background pixels (again...)
for (int j=0; of && j<size; ++j) {
    bool inFg = fgMask.getPixel(j);
    if (inFg) {
        Pixel i=image.getPixel(j);
        // compute image location and distance from centre:
        IPoint p(j%image.width(),j/image.width());
        IPoint d=p-v.spot.center;
        // normalized radius
        double r=sqrt(d.x()*d.x()+d.y()*d.y())/v.spot.radius;
        // normalized pixel intensity (just for the profile)
        double z=(i->foreground[c])/sqrt(i->fgvariance[c]);
        of << r << '\t' << z << endl;
    }
}
of.close();

```

Figure 3: Key modification of `dqmain.cc` in the Dapple source code package, detailing extraction and normalization of pixel intensities. The code is inserted at the end of function `DappleQuantifier::computeQuantStats`.

Algorithm and Implementation

The C++ spot finding program Dapple has been extended to perform the first step of the analysis. To allow a comparison of profile shapes between spots of different sizes and mean intensities, for each spot k , the raw intensities of all pixels l were normalized to $(I_{kl} - \mu_k)/\sigma_k$, with $(\mu, \sigma)_k$ being their arithmetic mean and standard deviation, respectively. Radial distances – pixel to spot centre – were computed and scaled to the range $0 \dots 1$. The standardized pixel intensities and radial distances for both fluorescence channels (Cy3/Cy5) were processed and stored independently. For precision, the code for pixel intensity extraction and normalization is shown in Fig. 3.

The statistical programming environment R (<http://www.r-project.org/>) and the Loess implementation of its *modreg* package were used to calculate a Loess interpolation of average pixel intensity as a function of radial distance. The local population standard deviation from this average was then computed using a Loess smoother. This is a measure of both the deviation from radial symmetry in individual spots, and the variance of shape across spots of a subgrid. All Loess interpolation was performed with the default parameters and an approximation for the trace of the smoother matrix as recommended for data sets of the size encountered (c.f. *modreg* online documentation).

The resulting coefficients of variation, with respect to the radial distance, or to the set of spot pixels, were both used in combination with visual as-

assessment of the profile shapes to select advantageous buffer / slide combinations. Tables of all results are available in the Supplement. Data from individual subgrids and channels were analysed independently to separate confounding factors.

Discussion and Conclusion

Analysis of radial spot pixel intensity profiles proved to be remarkably reproducible, with no obvious differences between the two replicates of each slide type. Altogether, an extremely wide range of spot morphologies was observed. Spot sizes ranged from $< 60 \mu\text{m}$ for 1.5 M betaine with 10% DMSO on SuperAmine slides to $180 - 230 \mu\text{m}$ for 50% DMSO with 0.01% sarkosyl on PLL slides. Some of the more striking shapes are shown in Fig. 4 [2–3], including the classical ‘doughnut’ thoroughly analysed by Tran *et al.* (2002). Other malformations, resembling ‘fried eggs’, have an intensity profile marked by deviation from radial symmetry that is reflected in the extremely high variances. This asymmetry arises within the spot, in contrast to spots with asymmetrical boundaries (Fig. 2b). Figure 4 [4–8] also displays the range of effects observed when changing the slide type for a given buffer, varying the buffer on a specific slide type, and of printing with different pins for a given buffer / slide combination. It is noteworthy that some combinations gave very different responses in the two fluorescence channels, e.g., 30% DMSO on slides by Corning and Apogent (Fig. 4 [1]). To a lesser degree, however, many buffer / slide combinations exhibited channel specific effects. This puzzling observation has not been pursued further.

The selection of an ideal printing buffer is driven by several criteria, an important one being the minimization of all the above forms of variance. Other issues include acceptable signal intensity and, particularly when printing high-density arrays, the requirements of low buffer evaporation rates and short pin washing times. Uncertain readings from tiny spots limit practical spot size.

Here, we present only the highest ranking buffer/slide combinations of our survey. Comprehensive results are found in the Supplement. By far the best average profile shape and low variance on all accounts, one of the slowest evaporation rates, and negligible carry-over with short pin wash cycles were achieved using a buffer of 50% DMSO and 0.1% PEG on FMB cDNA slides, yielding spots of average size $(118 \pm 2) \mu\text{m}$, with minimum discernible rush (Fig. 2a). The second ranking combination was $3\times$ SSC with 1.5 M betaine plus 5% DMSO on in-house PLL, GAPS II, Ultra GAPS, and SuperAmine slides (in that order). The buffer is hence very versatile. The spots have a tolerably good shape (a bell shape, see Fig. 4 [4]), variances are fairly low, typical spot size is $130 \mu\text{m}$ (SuperAmine: $118 \mu\text{m}$) and the buffer evaporates at a moderate speed. For the buffer tested by Diehl *et al.* (2001), $3\times$ SSC with 1.5 M betaine, a comparably good performance was achieved on the Corning slides ($130 \mu\text{m}$ spots); profile variances were lower on Ultra GAPS than on GAPS II. The buffer is, however, less versatile, and evaporates faster.

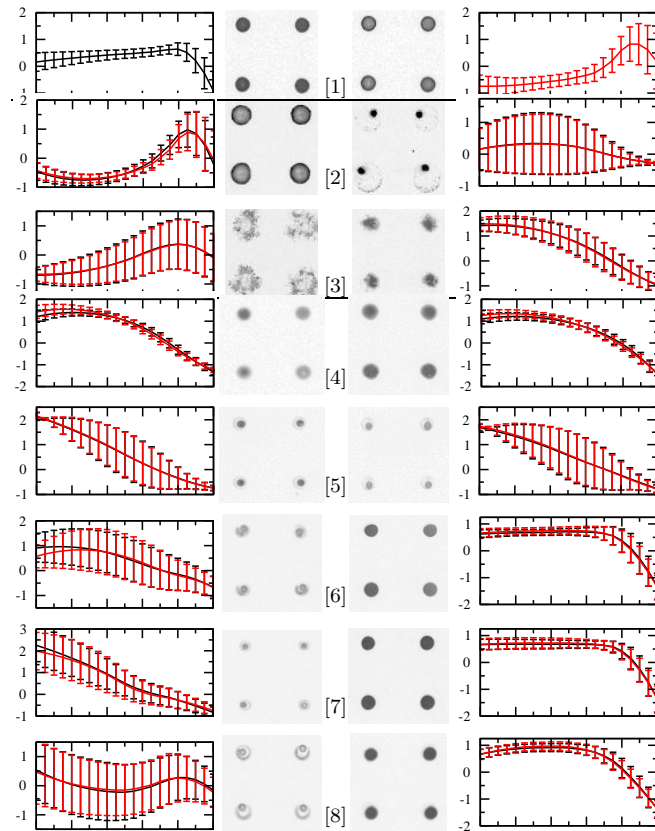


Figure 4: Radial intensity profile analysis. L=left, R=right subpanel.

[1] Dye specific response, shown for 30% DMSO on Ultra GAPS: [1L] Cy3 channel. [1R] Cy5 channel.

[2–3] Spot malformation examples, shown for PLL slides: [2L] ‘doughnuts’ – 30% DMSO with 0.01% sarkosyl; [2R] ‘fried eggs’ – 3× SSC with 1% PEG; [3L] ‘spat spots’ – 3× SSC with 1% PPG; [3R] non-round spots – 3× SSC with 1% glycerol plus 0.01% sarkosyl.

[4–8] **a.** The effect of slide chemistries, shown for 3× SSC with 1.5 M betaine plus 5% DMSO: GAPS II [4L] and PLL slides [4R] are similar, yet GAPS II [4L] and FMB cDNA slides [5L] differ. **b.** The effect of buffer chemistries, shown for FMB cDNA slides: 3× SSC with 1.5 M betaine plus 5% DMSO [5L], and 1.5 M betaine with 10% DMSO [5R] are similar, whereas 3× SSC with 1.5 M betaine plus 5% DMSO [5L], and 50% DMSO with 0.1% PEG [6–8R] differ. **c.** Pin-to-pin variability: [6–8L] High variability – 150 mM NaPO_4 with 0.01% SDS on SuperAmine slides. [6–8R] Very low variability – 50% DMSO with 0.1% PEG on FMB cDNA slides.

Unless specified otherwise, spot images are from the Cy3 channel.

Eventually, a robust parametric fit of realistic spot models to spot image data should provide us with much better signal estimators. With the constraints of the flat disc model removed, $3\times$ SSC with 1.5 M betaine plus 5% DMSO might become an even more attractive choice.

References

- Balagurunathan, Y., Dougherty, E.R., Chen, Y., Bittner, M.L., and Trent, J. (2002) Simulation of cDNA microarrays via a parameterized random signal model. *J. Biomed. Opt.*, **7**(3), 507–523.
- Baldi, P. and Long, A.D. (2001) A Bayesian framework for the analysis of microarray expression data: regularized *t*-test and statistical inferences of gene changes. *Bioinformatics*, **17**(6), 509–519.
- Brown, C.S., Goodwin, P.C., and Sorger, P.K. (2001) Image metrics in the statistical analysis of DNA microarray data. *Proc. Natl. Acad. Sci. U. S. A.*, **98**(16), 8944–8949.
- Buhler, J., Ideker, T., and Haynor, D. (2000) Dapple: Improved techniques for finding spots on DNA microarrays. *Technical Report*, UWTR 2002-08-05, University of Washington, Seattle, U. S. A.
- Diehl, F., Grahlmann, S., Beier, M., and Hoheisel, J. (2001) Manufacturing DNA microarrays of high spot homogeneity and reduced background signal. *Nucleic Acids Res.*, **29**(7), e38.
- Efron, B. and Tibshirani, R. (2002) Empirical bayes methods and false discovery rates for microarrays. *Genet. Epidemiol.*, **23**(1), 70–86.
- Kreil, D.P. and MacKay, D.J.C. (2003) Reproducibility assessment of independent component analysis of expression ratios from DNA microarrays. *Comparative and Functional Genomics*, **4**(3), 300–317.
- Lönnstedt, I. and Speed, T. (2002) Replicated microarray data. *Statistica Sinica*, **12**, 31–46.
- Long, A.D., Mangalam, H.J., Chan, B.Y., Toller, L., Hatfield, G.W., and Baldi, P. (2001) Improved statistical inference from DNA microarray data using analysis of variance and a Bayesian statistical framework. Analysis of global gene expression in *Escherichia coli* K12. *J. Biol. Chem.*, **276**(23), 19937–19944.
- Tran, P.H., Peiffer, D.A., Shin, Y., Meek, L.M., Brody, J.P., and Cho, K.W.Y. (2002) Microarray optimizations: increasing spot accuracy and automated identification of true microarray signals. *Nucleic Acids Res.*, **30**(12), e54.
- Tusher, V.G., Tibshirani, R., and Chu, G. (2001) Significance analysis of microarrays applied to the ionizing radiation response. *Proc. Natl. Acad. Sci. U. S. A.*, **98**(9), 5116–5121.
- Yang, Y.H., Buckley, M.J., and Speed, T.P. (2001) Analysis of cDNA microarray images. *Brief. Bioinform.*, **2**(4), 341–349.